SUPPORTING INFORMATION

Rational design and synthesis of Co(II), Ni(II) and Cu(II) complexes bearing 1,2,4-triazole scaffold for biological applications

Azza A. Hassoon[a]*, Hamada S. Abulkhair[bc], Ranim H. Ashour[d], Mariam M. Abdelsamea[d], Haidy O. Abdullah[d], Mona A. Eldesoky[d], Ali R. Shaban[d], Philopater John[d], Eslam A. Ghaith[ae]

[a] *Chemistry Department, Faculty of Science, Mansoura University, Mansoura 35516, Egypt*
[b] *Pharmaceutical Organic Chemistry Department, Faculty of Pharmacy, Al-Azhar University, Nasr City 11884, Cairo, Egypt*
[c] *Pharmaceutical Chemistry Department, Faculty of Pharmacy, Horus University-Egypt, International Coastal Road, New Damietta 34518, Egypt*
[d] *Forensic Science Program, Faculty of Science, New Mansoura University, New Mansoura 35712, Egypt*
[e] *Chemistry Department, Faculty of Science, New Mansoura University, New Mansoura 35712, Egypt*

Corresponding author: azza_ahmed@mans.edu.eg

1 Experimental

1.1. Materials and Methods

Utilized chemicals and solvents in the current paper were of highest purity; $CoCl_2.6H_2O$, $NiCl_2.6H_2O$, $CuCl_2.4H_2O$, dimethylsulphoxide (DMSO), diethyl ether (BDH or Merck), MeOH, nitric acid (Aldrich).

1.2. Instruments

Infra-red spectra utilizing KBr discs were recorded on Bruker IFS-66 FTIR Spectrometer. Chloride ions were calculated gravimetrically using the AgCl precipitate by utilizing $AgNO_3$ as precipitating agent. The melting or decomposition temperatures of complexes were measured in an electro-thermal melting point instrument. The electronic conductance was measured in DMSO with conductivity meter at room temperature. Elemental analyses of the complexes for (Carbon, Hydrogen, Nitrogen and Sulfur) were carried out by micro-analytical Services at Mansoura University. UV2 Unicam spectrophotometer (200–1100 nm) recorded the electronic spectra. Thermogravimetric analyses (TGA, DTA, 20-700°C) was carried out with Shimadzu TGA-50 analyzer. The magnetic susceptibility values were calculated using the relation $\mu_{eff} = 2.83(\chi_m.T)^{1/2}$. The diamagnetic corrections were made by Pascal's constant and $Hg[Co(SCN)_4]$ was used as a calibrant. Bruker EMX spectrometer was used to obtain ESR spectra. Mass spectra were obtained on a Shimadzu GC/MS-QP5050A mass spectrometer. The ^1H and ^{13}C NMR spectra were recorded on JEOL ECA II (500 M*Hz)* using DMSO-d_6 as the solvent.

1.3. Biological studies

1.3.1. Determination of cytotoxic and antimicrobial activities

HeP-2, HePG2, MCF-7, and HeLa cell lines, derived from the mammary gland were acquired from ATCC through VACSERA, a biological products and vaccines holding company based in Cairo, Egypt. The cell lines were utilized to assess the inhibitory impact of substances on cell proliferation by the MTT test. This colorimetric assay relies on the transformation of the yellow tetrazolium bromide (MTT) into a purple formazan derivative by mitochondrial succinate dehydrogenase in living cells. The cell line was grown in RPMI-1640 media supplemented with 10% fetal bovine serum. The antibiotics used were 100 units/ml of penicillin and 100 µg/ml of streptomycin, incubated at 37°C in a 5% CO_2 environment. The cell line was cultured in a 96-well

plate with a density of 1.0 x 10^4 cells/well at 37°C for 48 hours in a 5% CO_2 environment. Following incubation, the cells were exposed to varying concentrations of complexes and incubated for 24 hours. After 24 hours of drug treatment, 20 microliters of MTT solution at a concentration of 5 milligrams per milliliter was added and incubated for 4 hours. 100 µl of Dimethyl sulfoxide (DMSO) is added to each well to dissolve the purple formazan. The colorimetric assay is quantified at an absorbance of 570 nm using a plate reader (EXL 800, USA). The percentage of relative cell viability was determined using the formula: (A570 of treated samples/A570 of untreated sample) X 100. All the experiments were carried out in triplicate and IC_{50} values were expressed as mean ± SD.

The synthesized compounds were evaluated for their antimicrobial activity against Staphylococcus aureus (gram-positive bacteria) and Escherichia coli (gram-negative bacteria). Furthermore, the compounds were investigated for their antifungal properties against Candida albicans. Each compound was dissolved in DMSO to generate separate solutions with a concentration of 1 mg/ml. Paper discs made of Whatman filter paper were cut to a standard size of 5 cm and sterilized in an autoclave. The paper discs, saturated with the specified concentration of the complex solution, were aseptically positioned on petri dishes filled with nutrient agar media (consisting of agar 20 g, beef extract 3 g, and peptone 5 g) inoculated with Staphylococcus aureus, E. coli, and Candida albicans. The petri plates were placed in an incubator set at 36 degrees Celsius, and the inhibition zones were measured 24 hours later. Each treatment was duplicated thrice. The antibacterial properties of the conventional antibiotic Ciprofloxacin and antifungal Colitrimazole were tested using the same method, concentration, and solvents as previously described. The activity index for the complex was determined using the following formula:

$$\%\ Activity\ Index = \frac{Zone\ of\ inhibition\ by\ test\ compound\ (diametre)}{Zone\ of\ inhibition\ by\ standard\ (diametre)} \text{x100}$$

1.3.2. Flow cytometry (Apoptotic and cell cycle arrest) assay

i. Cell cycle analysis

The IC_{50} of **Ni-AHMT** complex was added to seeded MCF-7 cell lines, respectively in four six well plates. The first three wells from each plate were treated with the IC_{50} of the complex and the last 3 wells will be the control wells without treatment. The DNA content of MCF-7 cell treated with the complex by cell cycle progression were evaluated. The cells were harvested, washed twice

with 1 mL buffer solution, centrifuged for 5 min at room temperature, then the supernatant was removed. The treated and untreated cell were re-suspended in 200 μL PBS. Then, the cells were fixed in 5 mL of ice-cold 70 % ethanol at 4 ^{o}C overnight and stained with 100 μL PI/RNase solution (0.1 mg/mL PI containing 1 mg/mL RNase A) for 30 min at room temperature in dark. The stained cells were analyzed tropically.

ii. Apoptotic assay

The apoptosis assay of **Ni-AHMT** complex was performed by annexin V-FITC/ PI (propidium iodide) analysis using apoptosis detection kit (K101, Biovision) in MCF-7 cells by flow cytometry. The cell, MCF-7 was cultivated after treatments with the complex (at IC_{50} μM) for 24 h. Then, the cells were collected by centrifugation and re-suspended in 500 μL of 1X binding buffer (0.1 M HEPES/NaOH (pH 7.4), 1.4 M NaCl, 25 mM $CaCl_2$). In dark, a number of 1×10^5 cells were mixed with 5μL of Annexin V-FTIC and 5μL of PI for 15 min at room temperature. The data (early, late apoptosis or necrosis were analyzed as a percentage of all cells flow cytometer (BD FacScan Flowcytometry, USA).

1.3.3. DNA binding

Methyl green reversibly binds to DNA, and the coloured complex is stable at neutral pH, whereas free methyl green fades at this pH value. DNA- binding active compounds displace DNA from its methyl green complex. The displacement was determined by a spectrophotometric assay as a decrease in the absorbance at 630 nm.

DNA methyl green (20 mg) was suspended in 100 ml of 0.05 M Tris-HCl buffer (pH 7.5) containing 7.5 mM $MgSO_4$; the mixture was stirred at 37 °C with a magnetic stirrer for 24 h. Test samples (10,100,1000μg) were dissolved in ethanol in Ependoff tubes, solvent was removed under vacuum, and 200μl of the DNA/methyl green solution were added to each tube. Samples were incubated in the dark at ambient temperature. After 24 h, the final absorbance of the samples was determined at 642.5-645 nm. Readings were corrected for initial absorbance and normalized as the percentage of the untreated standard.

1.3.4. Determination of SOD-like activity

Superoxide dismutase (SOD)-like activity was investigated using Bridges and Salin method. This method is based on the inhibitory effect of SOD on the reduction of nitrobluetetrazolium (NBT) by the superoxide anion generated by the xanthine/xanthine oxidase system.

1.3.5. Antioxidant activity assay by DPPH model

The free radical scavenging activity of the compounds was measured by DPPH method. The reaction mixture of synthesized compounds at different concentration aliquots was taken and the volume was adjusted up to 3mL with methanol. To this mixture 1 mL of 0.1 mM solution of DPPH in methanol was added. The mixture was kept in the dark for 30 min. The free radical scavenging activity of synthesized compounds was compared with standard Butylated Hydroxytoluene (BHT). Optical density was measured at 517 nm and the inhibition of concentration was calculated. One milliliter of 0.1 mM of methanolic solution of DPPH and 3 mL of methanol was considered as control.

$$\% \text{ of inhibition} = [(A_{cont} - A_{test}) A_{cont}] \times 100$$

where A_{cont} is the absorbance of control and A_{test} is the absorbance of the test sample. The sample concentration providing 50% inhibition (IC_{50}) was determined. All the experiments were carried out in triplicate and IC_{50} values were expressed as mean ± SD.

1.4. Molecular Docking

The crystal structure of the doubly stranded DNA (PDB ID: 1D66; https://www.rcsb.org/structure/1D66) has been retrieved from the Research Collaboratory for Structural Bioinformatics Protein Data Bank (RCSB PDB) [1]. Similarly, the crystal structures of β-lactamase (PDB ID: 4OQG; https://www.rcsb.org/structure/4OQG) and HSA (PDB ID: 2BXD; https://www.rcsb.org/structure/2BXD) were retrieved [2,3]. For each crystal structure, the solvent and other binding molecules were removed; polar hydrogens were added, and missing amino acid residues were constructed. 3D structures with minimized energies of **AHMT** and its complexes with Co(II), Ni(II), and Cu(II) have been generated with ChemDraw software for subsequent docking. The docking experiments were conducted applied and validated by redocking assessing an RMSD value to be ≤ 2.00 Å as previously reported [4–7].

Docking protocol and validation

Prior to docking, the target macromolecules (DNA double helix*, E. coli* β-lactamase, and Human Serum Albumin) were prepared by removing crystallographic water molecules, adding polar hydrogens, and minimizing energy using the MMFF94x forcefield. Molecular docking studies were performed using the Molecular Operating Environment (MOE) software. Ligand placement was achieved using the Triangle Matcher algorithm, and binding poses were initially scored using the London *d*G scoring function. The top-ranked poses were subsequently refined by force-field-based optimization and rescored using the GBVI/WSA *d*G function to estimate binding free energies [8]. For each ligand, the most energetically favorable and geometrically reasonable pose was selected for further analysis. The docking grid was defined to fully encompass the biologically relevant binding regions of each target, including the base-pair region of the DNA duplex, the catalytic pocket of β-lactamase, and Sudlow site I of HSA. Grid dimensions and positioning were selected to allow sufficient flexibility for ligand accommodation while maintaining target specificity. Docking pose reliability was evaluated by monitoring RMSD values, with poses displaying RMSD values below 2.0 Å considered acceptable [9, 10].

To validate the adopted protocol and pocket selection, reference ligands were employed where appropriate. In particular, warfarin was redocked into the HSA binding site, reproducing its reported binding mode and key interactions with residues Tyr150, Lys199, and Arg222 [3], thereby confirming the reliability of the docking setup. Similarly, the co-crystallized ligand of *E. coli* β-lactamase (2UL) was re-docked, and the obtained results was compared to reported binding mode and key interactions (Ala237, Asn170 and Asn132) to validate results [2]. All docking results were analyzed based on binding scores, RMSD values, and hydrogen bonding, electrostatic, π–π, and hydrophobic interactions.

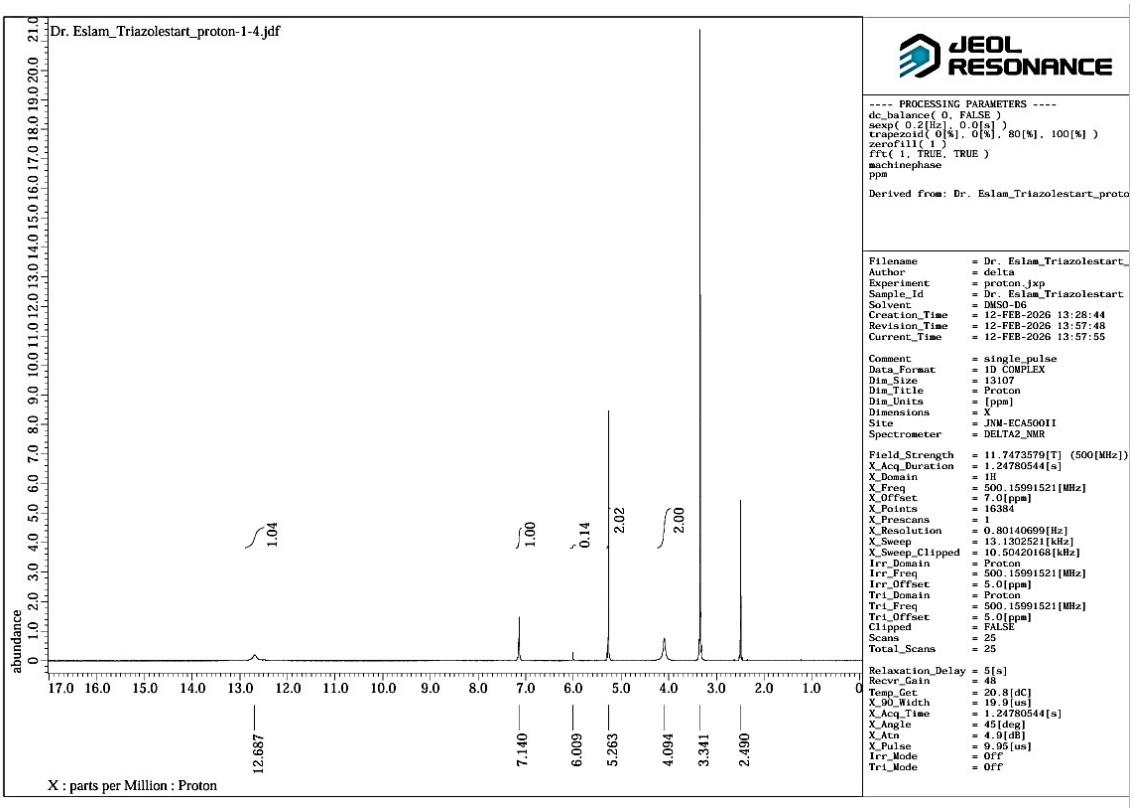

Fig. S1. ^{1}H-NMR spectrum of studied ligand (**AHMT**) in d_6-DMSO.

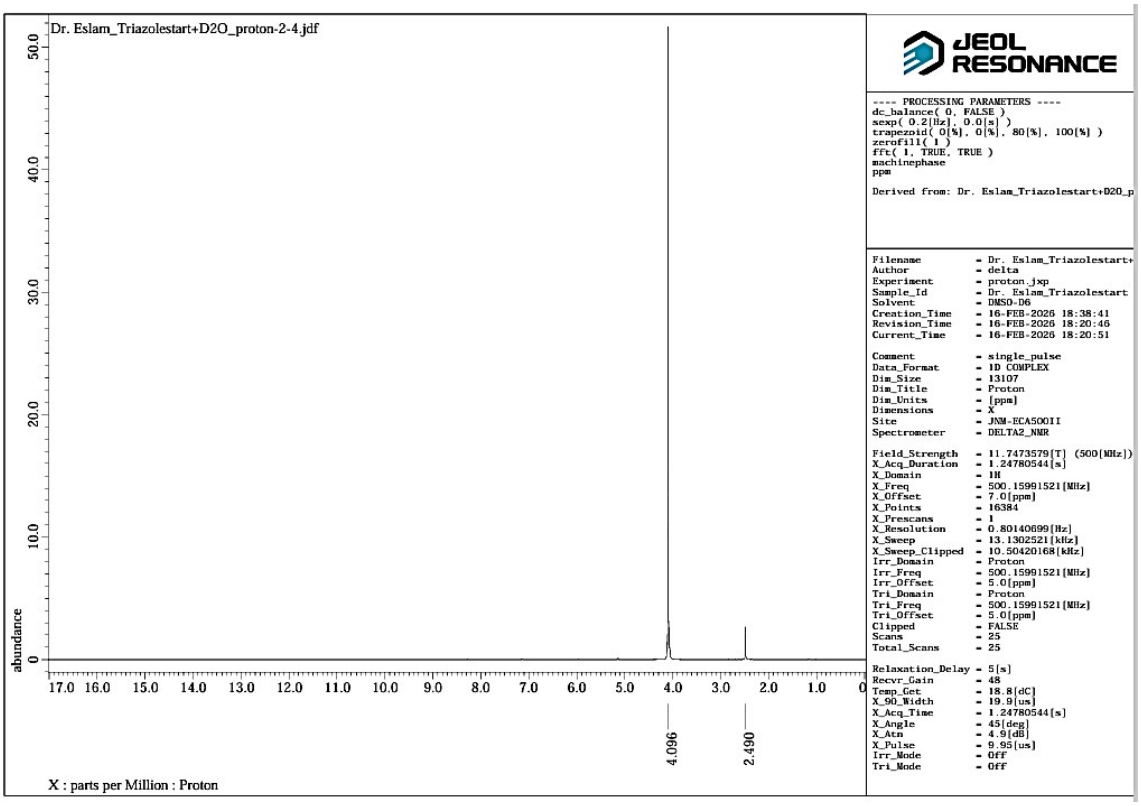

Fig. S2. ^{1}H-NMR spectrum of studied ligand (**AHMT**) in D_2O.

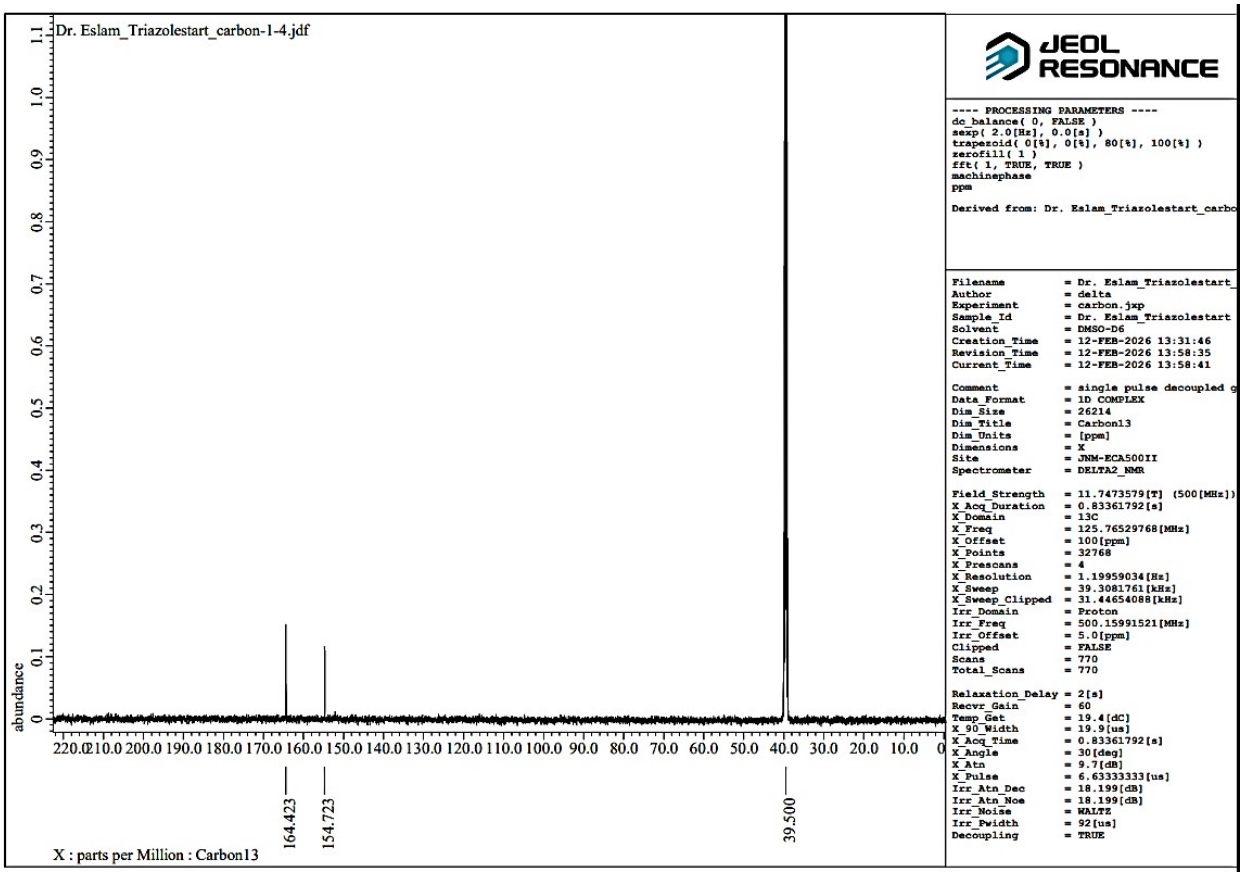

Fig. S3. ^{13}C-NMR spectrum of studied ligand (**AHMT**).

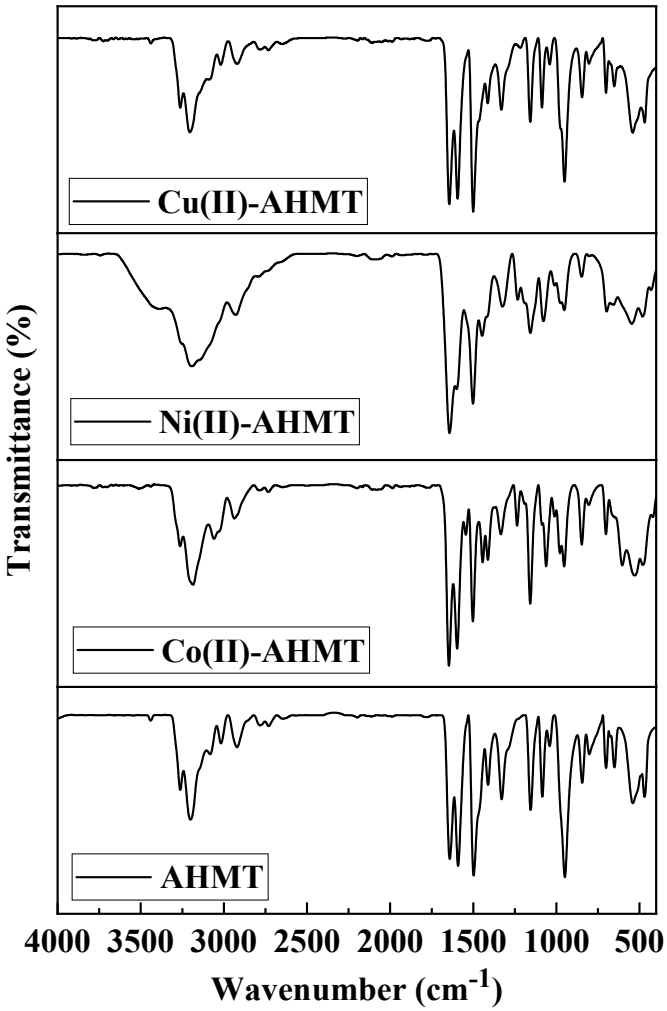

Fig. S4. IR spectrum of studied ligand (**AHMT**) and its metal complexes.

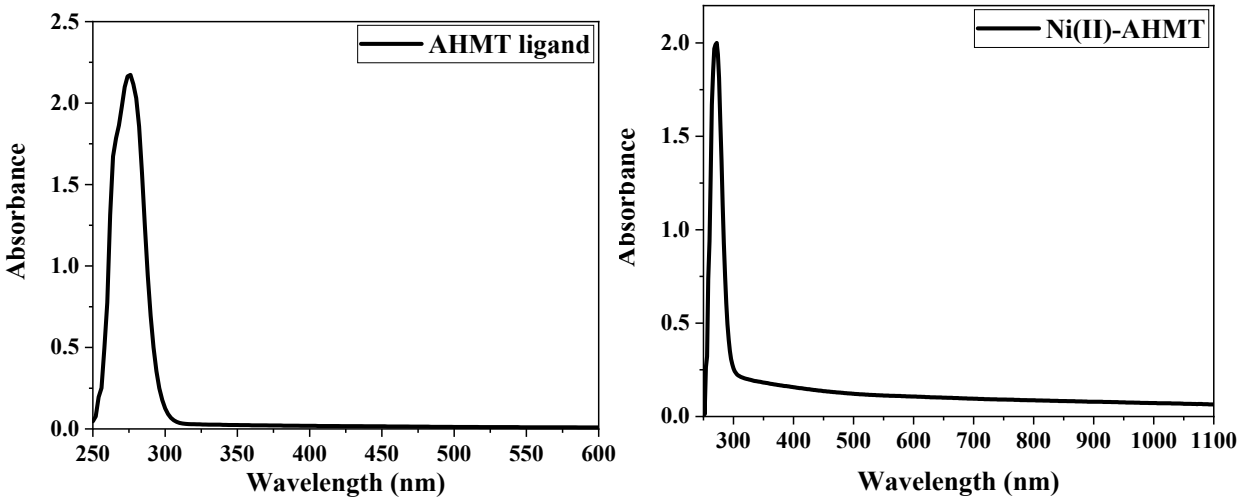

Fig. S5. Electronic spectra of **AHMT** and **Ni(II)-AHMT complex**.

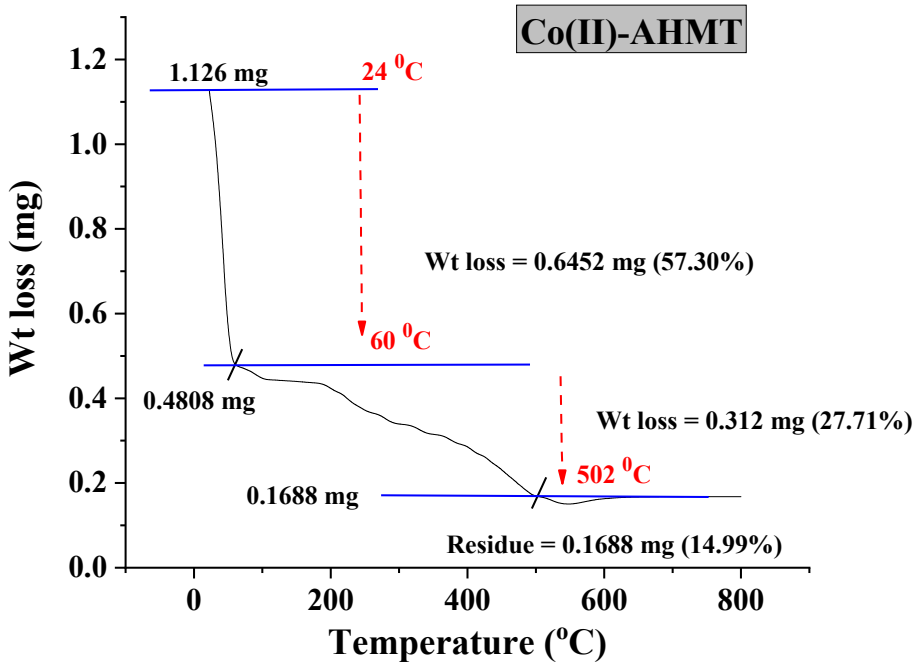

Fig. S6. The TGA curve of **Co(II)-AHMT** complex.

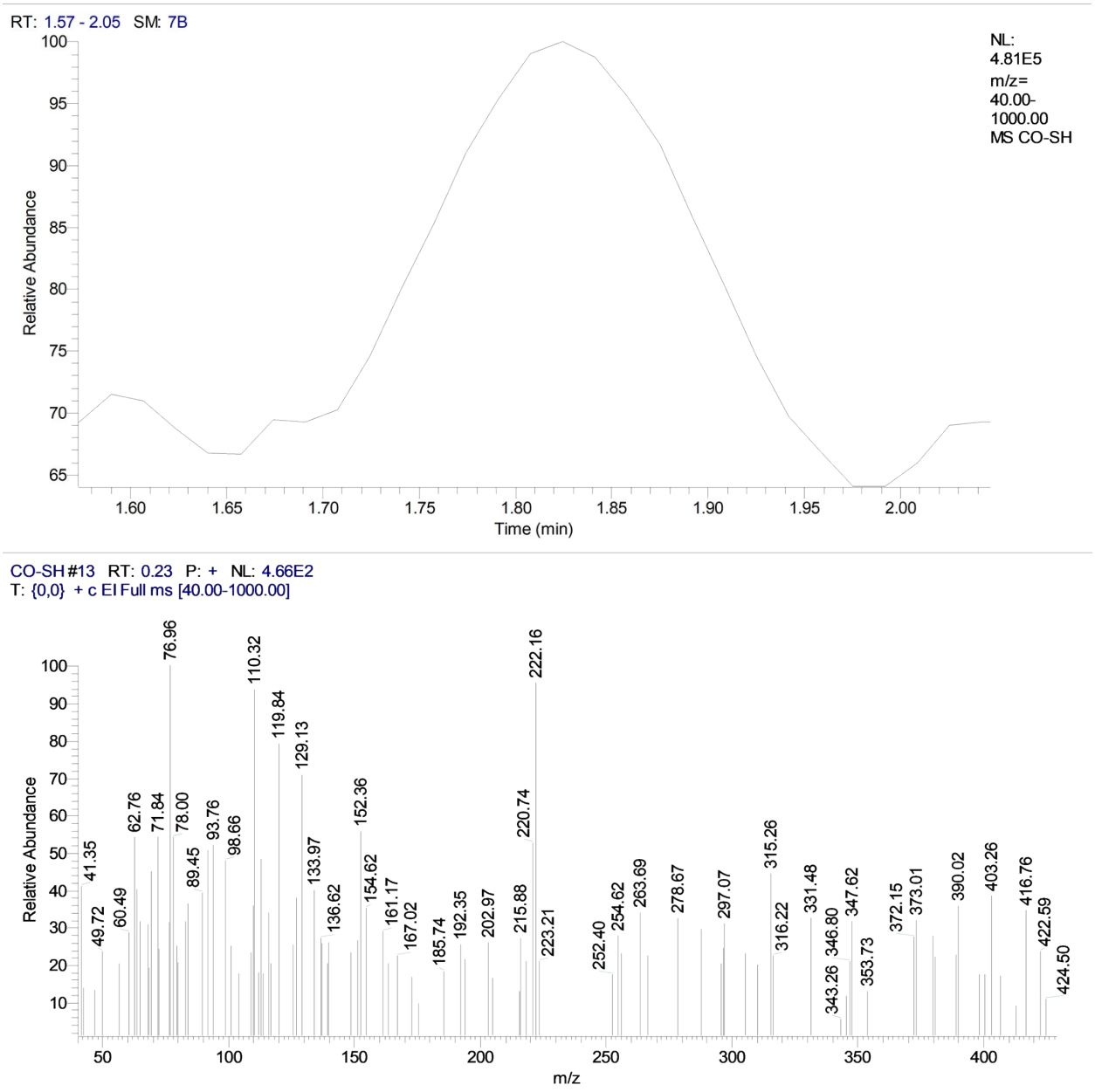

Fig. S7. Mass spectrum of **Co(II)-AHMT**

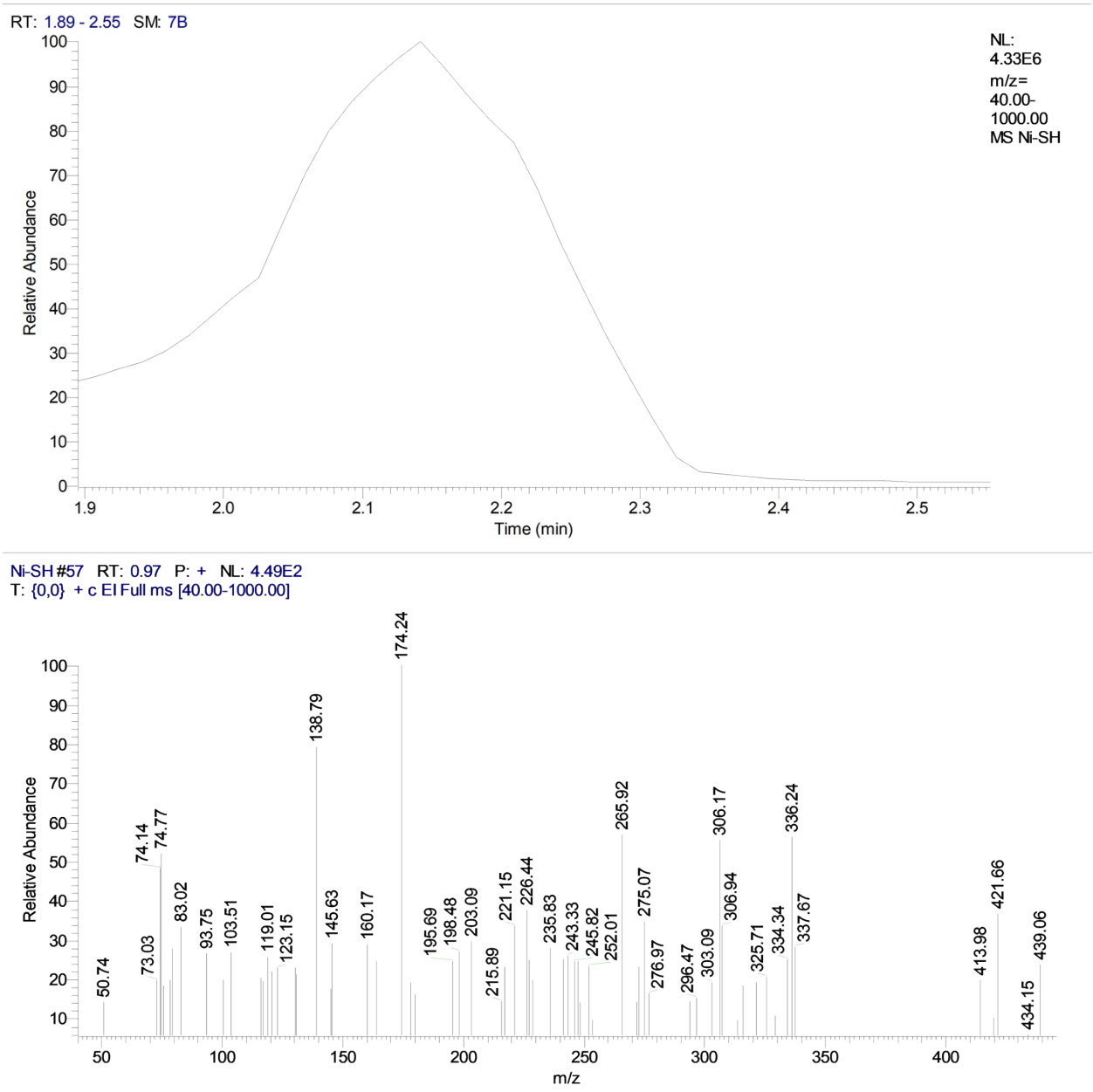

Fig. S8. Mass spectrum of **Ni(II)-AHMT**

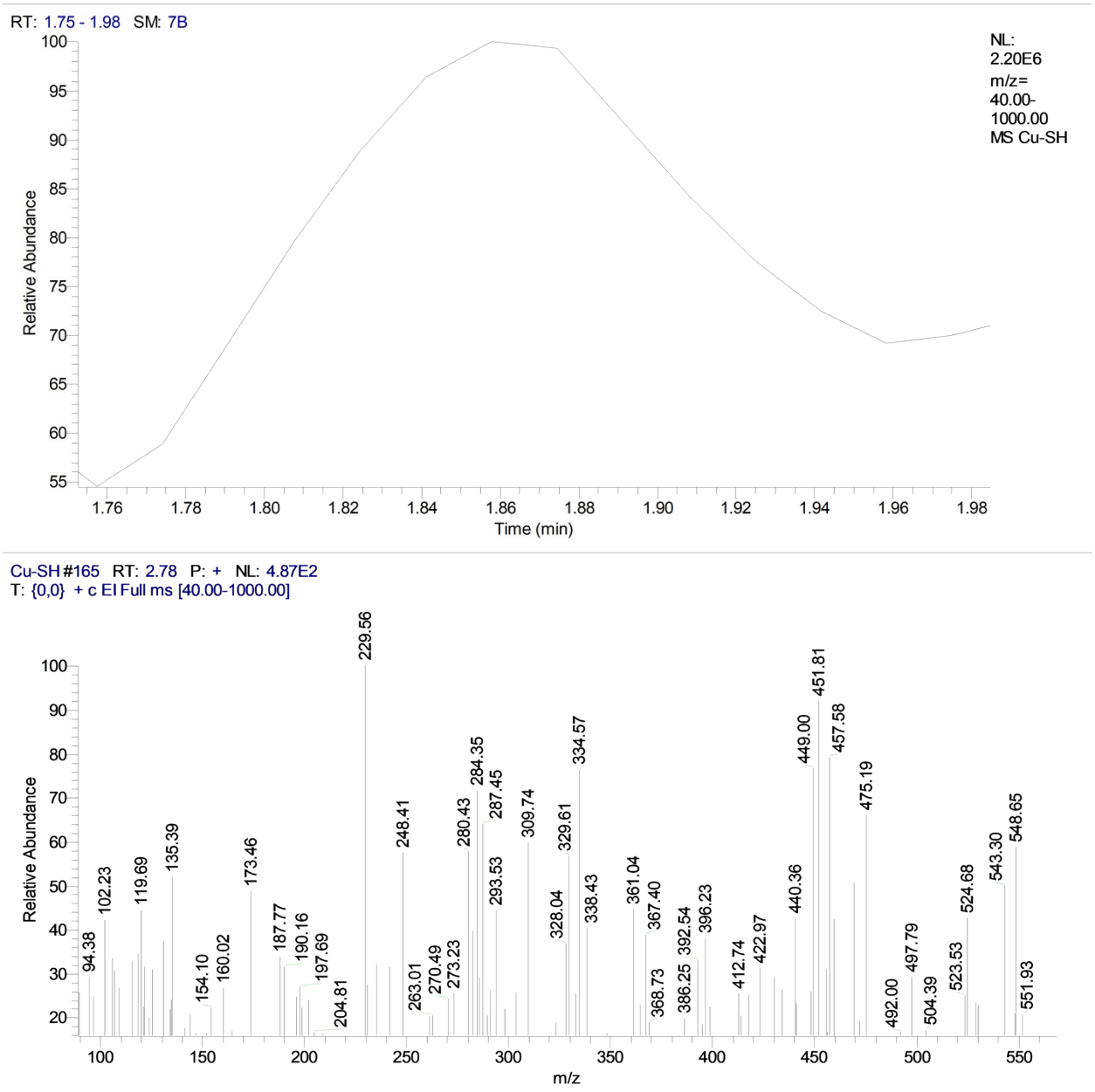

Fig. S9. Mass spectrum of **Cu(II)-AHMT.**

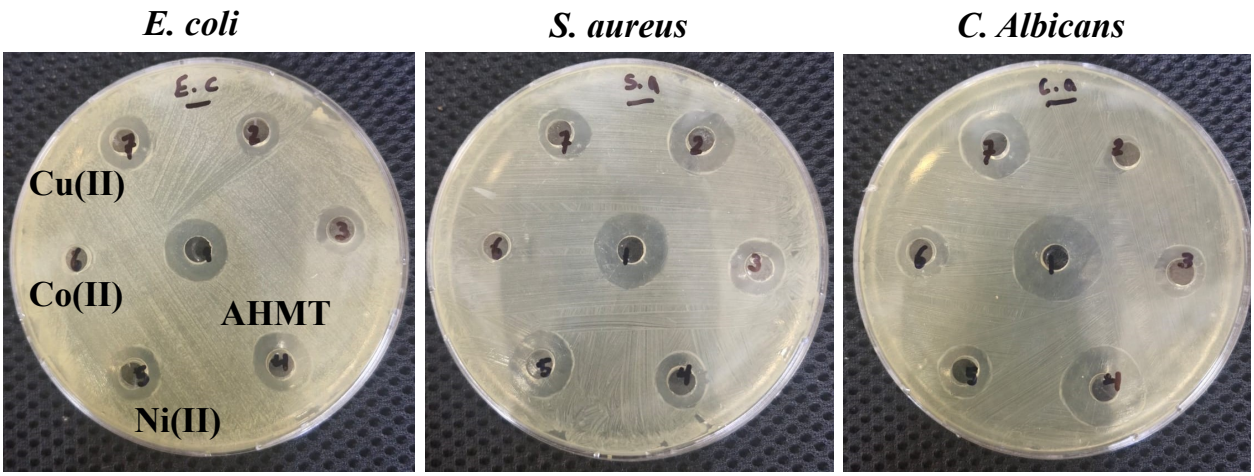

Fig. S10. Antimicrobial activity of **AHMT** ligand and its metal complexes against *E. coli*, *S. aureus*, and *C. albicans*. The images show the representative clear zones of inhibition (ZOI) obtained by the disc diffusion method.

Table S1. Antimicrobial activities of **AHMT** and its isolated metal complexes.

Compound	*E. coli*		*S. aureus*		*C. Albicans*	
	Diameter of inhibition zone (mm)	**% Activity index**	**Diameter of inhibition zone (mm)**	**% Activity index**	**Diameter of inhibition zone (mm)**	**% Activity index**
AHMT	9	34.6	11	45.8	16	59.2
Co(II)-AHMT	3	11.5	5	20.8	8	29.6
Ni(II)-AHMT	12	46.1	14	58.3	13	48.1
Cu(II)-AHMT	8	30.8	9	37.5	12	44.4
Ciprofloxacin	26	100	24	100	----	----
Colitrimazole	----	----	----	----	27	100

Table S2. MIC values of **AHMT** and its isolated metal complexes.

Compound	*E. coli*	*S. aureus*	*C. Albicans*
AHMT	8	16	4
Co(II)-AHMT	64	32	16
Ni(II)-AHMT	4	2	8
Cu(II)-AHMT	16	4	32
Ciprofloxacin	0.5	0.5	----
Colitrimazole	----	----	1

Table S3. *In vitro* Cytotoxicity IC_{50} (µM) ± SD* of **AHMT** and its complexes.

Comp.	In vitro Cytotoxicity IC_{50} (µM)					
	HePG-2	**MCF-7**	**HeP2**	**Hela**	**MCF-10A normal cells**	**SI (MCF-10A/MCF-7)**
DOX	4.50±0.2	4.17±0.2	8.54±0.6	5.57±0.4	2.51±2	0.6
SOR	9.18±0.6	7.26±0.3	10.22±0.7	8.04±0.5	….	…….
AHMT	18.01±1.4	15.50±1.2	26.27±1.6	21.46±1.5	110±0.5	7.3
Co(II)-AHMT	53.27±3.1	42.84±2.6	64.48±3.6	49.77±2.9	95±2.8	2.2
Ni(II)-AHMT	24.76±1.6	8.70±0.5	32.80±2.1	9.72±0.7	124±4	14.3
Cu(II)-AHMT	40.62±2.5	28.18±1.7	55.58±3.2	34.74±2.2	98.8±1.6	3.5

(SI = IC_{50} normal/ IC_{50} cancer; n=3, $p<0.0001$ vs. Dox)

Table S4. Superoxide (SOD)-like activity of **AHMT** and its isolated its complexes.

Compound	Δ through 5 min	% inhibition
Control	0.450	0%
L-Ascorbic acid	0.098	78.2%
AHMT	0.109	75.8%
Co(II)-AHMT	0.311	30.9%
Ni(II)-AHMT	0.134	70.2%
Cu(II)-AHMT	0.257	42.9%

% inhibition = (ΔControl–ΔTest/ΔControl) x 100

Table S5. Antioxidant activity of **AHMT** and its isolated complexes

Comp.	**Conc (µM)**						
	10	**20**	**40**	**60**	**80**	**100**	**IC_{50}**
	% Inhibition						
Vit.C	38.7	52.1	69.6	81.8	87.4	94.5	16.81±0.10
AHMT	30.2	48.3	63.2	78.7	90.6	98.1	20.90±0.14
Co(II)-AHMT	13.7	21.8	32.1	46.3	57.0	69.8	62.05±0.48
Ni(II)-AHMT	27.1	38.7	55.1	69.0	79.6	92.8	27.81±0.19
Cu(II)-AHMT	21.5	35.4	50.2	65.1	72.5	89.3	33.51±0.22

Table S6. DNA/methyl green colorimetric assay of **AHMT** and isolated complexes.

DNA-active compound	**DNA/methyl green (IC_{50}, µM)**
DOX	31.54±1.5
AHMT	41.85±1.9

Co(II)-AHMT	71.13±2.8
Ni(II)-AHMT	38.32±1.7
Cu(II)-AHMT	57.60±2.2

Table S7. Docking scores, interacting residues, and types of interaction of **AHMT**, **Co(II)-AHMT**, **Ni(II)-AHMT**, and **Cu(II)-AHMT** with DNA.

Compound code	Score (Kcal/mol)	RMSD (Å)	Interacting nucleotide	Type of Interaction	Distance (Å)
AHMT	-4.21	1.92	DA10	H-donor	3.15
			DT31	H-donor	2.89
			DC32	H-donor	3.28
Co(II)-AHMT	-3.90	1.77	DG37	H-donor	2.93
			DG37	H-donor	3.17
			DA5	H-acceptor	2.94
			DG6	H-acceptor	3.97
Ni(II)-AHMT	-4.42	1.67	DG6	H-donor	3.00
			DG38	H-acceptor	4.22
			DG4	H-acceptor	4.19
			DG4	H-acceptor	3.29
			DA5	H-acceptor	3.58
			DG3	pi-H	4.44
Cu(II)-AHMT	-2.24	1.71	DA10	H-donor	2.99
			DT12	H-donor	3.31
			DC13	H-donor	3.60
			DC32	H-donor	3.42
			DT31	H-donor	3.36
			DT 31	pi-H	3.77

Table S8 Docking scores, interacting residues, and types of interaction of **AHMT**, **Co(II)-AHMT**, **Ni(II)-AHMT**, and **Cu(II)-AHMT** into the active pocket of *E. coli* β-lactamase.

Compound	Score (Kcal/mol)	RMSD (Å)	Interacting Residue	Type of Interaction	Distance (Å)
AHMT	-4.00	1.99	Gly236	H-acceptor	3.42
			Arg244	H-acceptor	3.51
			Tyr105	H-pi	3.47

			Ala237	pi-H	3.79
Co(II)-AHMT	-3.11	1.64	Met272 Glu104 Glu104 Glu240 Asn132 Tyr105	H-donor H-donor H-donor H-donor H-acceptor pi-pi	4.49 3.05 3.32 3.09 3.48 3.68
Ni(II)-AHMT	-5.77	1.88	Asn170 Glu166 Asn170 Ser130 Ser235 Arg244 Ala237	H-donor H-acceptor H-acceptor H-acceptor H-acceptor H-acceptor pi-H	3.10 2.81 2.95 3.59 2.77 2.56 4.48
Cu(II)-AHMT	-5.53	1.42	Glu104 Asn170 Glu104 Glu240 Met272 Glu104 Asn132 Glu104 Glu104 Glu240 Glu104 Glu104 Glu104	H-donor H-donor H-donor H-donor H-donor H-donor H-acceptor ionic ionic ionic ionic ionic ionic	3.17 3.10 2.68 3.34 3.91 3.02 3.51 3.70 2.68 3.34 3.38 3.20 3.02

Table S9 Docking scores, interacting residues, and types of interaction of **AHMT**, **Co(II)-AHMT**, **Ni(II)-AHMT**, and **Cu(II)-AHMT** into the active pocket of HSA.

Compound code	**Score (Kcal/mol)**	**RMSD (Å)**	**Interacting Residue**	**Type of Interaction**	**Distance (Å)**
AHMT	-4.63	1.41	Ser192 Lys195	H-donor pi-H	3.27 4.29

Co(II)-AHMT	-4.93	1.73	Ala291 Ile290 Lys195 Lys195 Lys199 Arg222 Lys199 Ala291	H-donor H-donor H-acceptor H-acceptor H-acceptor H-acceptor Ionic pi-H	2.99 3.21 3.43 4.09 2.71 2.93 3.35 4.05
Ni(II)-AHMT	- 4.06	1.89	Lys195 Lys195 Lys199 Lys199 Ala291	H-acceptor H-acceptor H-acceptor Ionic pi-H	3.47 4.17 2.73 3.39 4.13
Cu(II)-AHMT	-2.51	1.58	Ala291 His242 Lys199 Arg222 His242	H-donor H-donor H-acceptor H-acceptor cation-pi	3.56 2.82 2.78 3.25 3.87

References

[1] R. Marmorstein, M. Carey, M. Ptashne, S.C. Harrison, DNA recognition by GAL4: structure of a protein-DNA complex, Nature 356 (1992) 408–414. https://doi.org/10.1038/356408a0.

[2] E. Dellus-Gur, M. Elias, E. Caselli, F. Prati, M.L.M. Salverda, J.A.G.M. de Visser, J.S. Fraser, D.S. Tawfik, Negative Epistasis and Evolvability in TEM-1 β-Lactamase—The Thin Line between an Enzyme's Conformational Freedom and Disorder, J. Mol. Biol. 427 (2015) 2396–2409. https://doi.org/10.1016/j.jmb.2015.05.011.

[3] J. Ghuman, P.A. Zunszain, I. Petitpas, A.A. Bhattacharya, M. Otagiri, S. Curry, Structural Basis of the Drug-binding Specificity of Human Serum Albumin, J. Mol. Biol. 353 (2005) 38–52. https://doi.org/10.1016/j.jmb.2005.07.075.

[4] E.M. Othman, E.A. Fayed, E.M. Husseiny, H.S. Abulkhair, Rationale design, synthesis, cytotoxicity evaluation, and in silico mechanistic studies of novel 1,2,3-triazoles with potential anticancer activity, New J. Chem. 46 (2022) 12206–12216. https://doi.org/10.1039/d2nj02061k.

[5] A. Musa, S.K. Ihmaid, D.L. Hughes, M.A. Said, H.S. Abulkhair, A.H. El-Ghorab, M.A. Abdelgawad, K. Shalaby, M.E. Shaker, K.S. Alharbi, N.H. Alotaibi, D.L. Kays, L.J. Taylor, D.G.T. Parambi, S.I. Alzarea, A.A. Al-Karmalawy, H.E.A. Ahmed, A.M. El-Agrody, The anticancer and EGFR-TK/CDK-9 dual inhibitory potentials of new synthetic pyranopyrazole and

pyrazolone derivatives: X-ray crystallography, in vitro , and in silico mechanistic investigations, J. Biomol. Struct. Dyn. 41 (2023) 12411–12425. https://doi.org/10.1080/07391102.2023.2167000.

[6] S. Ihmaid, H.E.A. Ahmed, A. Al-Sheikh Ali, Y.E. Sherif, H.M. Tarazi, S.M. Riyadh, M.F. Zayed, H.S. Abulkhair, H.S. Rateb, Rational design, synthesis, pharmacophore modeling, and docking studies for identification of novel potent DNA-PK inhibitors, Bioorg. Chem. 72 (2017) 234–247. https://doi.org/10.1016/j.bioorg.2017.04.014.

[7] E.M. Husseiny, H. S. Abulkhair, N.M. El-Dydamony, K.E. Anwer, Exploring the cytotoxic effect and CDK-9 inhibition potential of novel sulfaguanidine-based azopyrazolidine- 3,5-diones and 3,5-diaminoazopyrazoles, Bioorg. Chem. (2023) 106397. https://doi.org/10.1016/j.bioorg.2023.106397.

[8] M. Wojciechowski and B. Lesyng, Generalized Born Model: Analysis, Refinement, and Applications to Proteins, *J. Phys. Chem. B*. 108 (2004) 18368–18376. https://doi.org/10.1021/jp046748b

[9] A. Saba, S. Muhammad, R. A. Khera, M. Alhujaily, J. Iqbal, A. R. Chaudhry, S. S. Alarfaji and T. M. Belali, Identification of Halogen-Based Derivatives as Potent Inhibitors of Estrogen Receptor Alpha of Breast Cancer: An In-Silico Investigation, *J. Comput. Biophys. Chem.*, 21 (2022) 181–205.

[10] H. S. Abulkhair, S. Elmeligie, A. Ghiaty, A. El-Morsy, A. H. Bayoumi, H. E. A. Ahmed, K. El-Adl, M. F. Zayed, M. H. Hassan, E. N. Akl and M. S. El-Zoghbi, In vivo- and in silico-driven identification of novel synthetic quinoxalines as anticonvulsants and AMPA inhibitors, *Arch. Pharm. (Weinheim).*, 354 **(**2021) 2000449. https://doi.org/10.1002/ardp.202000449